The Cryosphere Discuss., doi:10.5194/tc-2016-273, 2016
Manuscript under review for journal The Cryosphere
Published: 5 December 2016

The Cryosphere Discussions
Open Access
EGU

Arctic sea ice signatures: L-Band brightness temperature sensitivity comparison using two radiation transfer models

Friedrich Richter[1], Matthias Drusch[1], Lars Kaleschke[3], Nina Maaß[3], Xiangshan Tian-Kunze[3], and Susanne Mecklenburg[2]

[1]European Space Agency, ESA-ESTEC, 2200 AG Noordwijk, the Netherlands
[2]European Space Agency, ESA-ESRIN, Via Galileo Galilei, casella postale 64 - 00044, Frascati, Italy
[3]Institute of Oceanography, University of Hamburg, Bundesstraße 53, 20146 Hamburg, Germany

Correspondence to: Friedrich Richter (friedrich.richter@esa.int)

Abstract. Sea ice is a crucial component for short-, medium- and long term numerical weather predictions. Most importantly changes of sea ice coverage and areas covered by thin sea ice have a large impact on heat fluxes between the ocean and the atmosphere. L-Band brightness temperatures from ESA's first Earth Explorer SMOS (Soil Moisture and Ocean Salinity) have been proven to be a valuable tool to estimate mean thin sea ice thicknesses. Potentially, these measurements can be assimilated in forecasting systems to constrain the ice analysis leading to more accurate initial conditions and subsequently more accurate forecasts. As a first step, we use two different radiative transfer models as forward operators to generate top of atmosphere brightness temperatures based on ORAP5 model output for the 2012/2013 winter season. The simulations are then compared against actual SMOS measurements. The results indicate that both models are able to capture the general variability of measured brightness temperatures over sea ice. We identify one model to be favorable for brightness temperature assimilation purposes in the ORAP5 setup. The simulated brightness temperatures are dominated by sea ice coverage and thickness changes most pronounced in the marginal ice zone where new sea ice is formed. There we observe largest differences of more than 20 Kelvin over sea ice between simulated and observed brightness temperatures. We conclude that the assimilation of SMOS brightness temperatures yield high potential for forecasting models to correct for uncertainties in sea ice thicknesses of less than 0.5 meter and caution that uncertainties in sea ice fractional coverage may induce large errors.

1 Introduction

For the first time, the European Space Agency second Earth Explorer mission SMOS (Soil Moisture and Ocean Salinity) delivers brightness temperature measurements at 1.4 GHz on a global scale (Mecklenburg et al., 2012). SMOS L-Band brightness temperatures have been used to produce operational products of soil moisture over land (e.g. Albergel et al., 2011; Kerr et al., 2012) and ocean salinity over water areas (e.g. Reul et al., 2014) since 2010. Additionally, SMOS passive microwave imagery has been used to estimate sea ice parameters, such as sea ice thicknesses (e.g. Kaleschke et al. (2012), Tian-Kunze et al. (2014)), sea ice concentrations and snow coverage (Maaß et al., 2015). Microwave radiation is especially useful to derive thin sea ice thicknesses as it is able to penetrate snow and sea ice for more than half a meter and closes the gap to thicker sea ice thickness retrievals of more than 1 meter by using altimetry (Kwok and Cunningham, 2008; Kaleschke et al., 2010; Ricker et al., 2014;

The Cryosphere Discuss., doi:10.5194/tc-2016-273, 2016
Manuscript under review for journal The Cryosphere
Published: 5 December 2016

Tilling et al., 2016). This feature appears to be especially important since the Arctic Ocean is said to shift to a new state, in which older, thicker sea ice gets more and more replaced by younger and thinner ice (Laxon et al., 2013; Meier, 2015).

Much effort has been made to validate L-Band based sea ice thickness retrievals. In preparation for SMOS, Kaleschke et al. (2010) showed a significant agreement between sea ice thicknesses derived from L-band brightness temperatures and helicopter based electromagnetic induced (EM) sea ice measurements in the Bothnian Bay. After the launch of SMOS in 2009, the sea ice thickness retrieval has then been successfully validated with MODIS thermal infrared imagery data in the Kara and Lepedev sea (Kaleschke et al., 2012) and provided the first Arctic-wide map of thin sea ice thickness. The retrieval algorithm is based on the radiative transfer model of Menashi et al. (1993) and has been extended by a sea ice roughness approximation (Kaleschke et al., 2010), a thermodynamic sea ice model to consider variations of ice temperatures and ice salinities, as well as a sea ice thickness distribution (Tian-Kunze et al., 2014). Retrieved ice thicknesses prove to correlate with ship- and airborne observational thicknesses up to 1.5 m (Kaleschke et al., 2016). However, as previous algorithms lack a comprehensive representation of the complex structures of sea ice, such as electromagnetic properties from multiple sea ice layers and a snow layer on top, a second radiative transfer model was utilized, namely the model used in Maaß et al. (2013) a modified version of the multi-layer model from Burke et al. (1979). The model has been used to derive snow thicknesses over thick multi-year sea ice (Maaß et al., 2013) but has not yet been applied to derive sea ice thicknesses on an Arctic-wide scale.

A valuable application for sea ice observations is the assimilation into forecasting models. The assimilation of fractional sea ice coverage derived by remote-sensing techniques has been proven to be very beneficial and is conducted in varies studies (e.g. Stark et al. (2008); Lindsay and Schweiger (2015)). The sea ice age derived from sea ice drift measurements from the National Snow and Ice Data Center (NSDIC) has been used as a proxy for sea ice thicknesses in the Arctic Sea Ice Volume reanalysis Pan-Arctic Ice Ocean Modeling and Assimilation System (PIOMAS) (Zhang and Rothrock, 2003). Those sea ice thicknesses were compared with observations from e.g. airplanes, buoys and submarines, but not on a larger scale. However, the direct assimilation of Arctic-wide remote-sensing based sea ice thicknesses has not yet been performed on a regular basis. As a first attempt, SMOS sea ice thicknesses of less than 0.4 m have been assimilated in the TOPAZ Arctic Ocean reanalysis with the result of reduced Root Mean Square Deviations (RMSD) between SMOS-Ice and TOPAZ reanalysis sea ice thicknesses in March and November (Xie et al., 2016). It has been found that the inconsistency between sea ice concentrations in SMOS and the model is one of the major limitations for a sea ice thickness assimilation. Furthermore, SMOS sea ice thicknesses have been assimilated into the Massachusetts Institute of Technology general circulation model (MITgcm) with a localized Singular Evolutive Interpolated Kalman (LSEIK) filter (Yang et al. 2014). They show that the assimilation leads to improved ice thickness forecasts, as well as better sea ice concentration forecasts.

To improve the accuracy of the sea ice thickness assimilation it is possible to consider other sea ice parameters, such as the sea ice fractional coverage or ice/snow surface temperatures. A common approach to do that is to assimilate brightness temperatures rather than a ready-to-use high-level satellite product. The advantage is the availability of a wide range of consistent input data, whereas independent sea ice thickness retrievals rely on assumptions, parameterizations and auxiliary data, such as climatologies or secondary reanalysis products. However, the question remains which radiative transfer model suits best to be used as a forward operator in a brightness temperature assimilation scheme for thin sea ice thicknesses. So far, simulated

The Cryosphere Discuss., doi:10.5194/tc-2016-273, 2016
Manuscript under review for journal The Cryosphere
Published: 5 December 2016

brightness temperatures have been validated for idealized typical Arctic conditions (e.g. Maaß et al. (2013), Tian-Kunze et al. (2014)), but have never been compared to L-Band remote sensing observations on a large scale.

In this study, we investigate the Arctic-wide performance of the radiative transfer models of Kaleschke et al. (2010) and Maaß et al. (2013) to account for diverse atmospheric and oceanic conditions and to identify the most important input parameters for a sea ice thickness application. In preparation for a brightness temperature assimilation, we concentrate on the input data of the global ocean reanalysis product ORAP5 (Ocean ReAnalysis Pilot 5) produced by the ECMWF. We evaluate which radiative transfer model to use for assimilating sea ice thickness into the ORAP5 reanalyses by comparing simulated and observed brightness temperatures from the radiative transfer models with ORAP5 input data and SMOS observations, respectively.

2 Data and Methods

Both radiative transfer models provide brightness temperatures as a function of temperature, snow- and sea ice thickness, incidence angle and the permittivity (Fig. 1). The latter is calculated with the snow, sea ice and sea water temperatures (as well as the snow/sea ice interface temperature), the bulk sea ice and water salinities and the snow and sea ice thicknesses. The sea ice salinity is estimated with the empirical approach of Ryvlin (1974) making the ice salinity a function of the sea surface salinity, the sea ice thickness, the salinity ration of the bulk ice salinity at the end of the sea ice growing season and the growth rate coefficient. The latter two are taken from Kovacs (1996) who derived a value of 0.175 for the ice salinity ration from observational data in the Arctic and 0.5 for the growth rate coefficient, as also suggested by Ryvlin (1974). To obtain the ice/snow interface we calculate the thermal conductivity of ice with the snow surface temperature and ice salinity (Untersteiner, 1964). Using this, we are able to determine the bulk sea ice temperature for our sea ice slab by assuming the heat fluxes are in equilibrium (Maykut and Untersteiner, 1971). We calculate the brine salinity with a polynomial approximation that uses bulk sea ice temperature (Vant et al., 1978; Leppäranta and Manninen, 1988) and the pure ice density as a function of bulk ice temperature (Pounder, 1965). As the polynomial coefficients for the brine salinity calculation are only provided for 1 and 2 GHz, we linearly interpolate between these two frequencies to determine the coefficients for 1.4 GHz. By taking the ice and brine density, as well as the bulk ice temperature, we are able to calculate brine volume fraction using equations valid for ice temperatures below -2°C from Cox and Weeks (1983) and above -2°C from Leppäranta and Manninen (1988). Finally, the permittivity of sea ice is derived by an empirical relationship to the brine volume fraction (Vant et al., 1978) (for a summary of references see table 1).

In order to represent sea ice brightness temperature measurements in partially covered data points over the open ocean, the models linearly include sea ice fractional coverage in the calculations for each grid cell. Additionally, both models consider the subpixel-scale heterogeneity of sea ice thicknesses with a statistical ice thickness distribution. We calculate the brightness temperatures for ten linearly divided sea ice thickness bins with a maximum of 2 meter thickness. Then, we translate the mean sea ice thickness from the input data to a sea ice thickness distribution derived by observational data (As used in Algorithm II* by Tian-Kunze et al. (2014)). The final brightness temperature is the average of the ten respective bins weighted by the sea ice thickness distribution.

The Cryosphere Discuss., doi:10.5194/tc-2016-273, 2016
Manuscript under review for journal The Cryosphere
Published: 5 December 2016

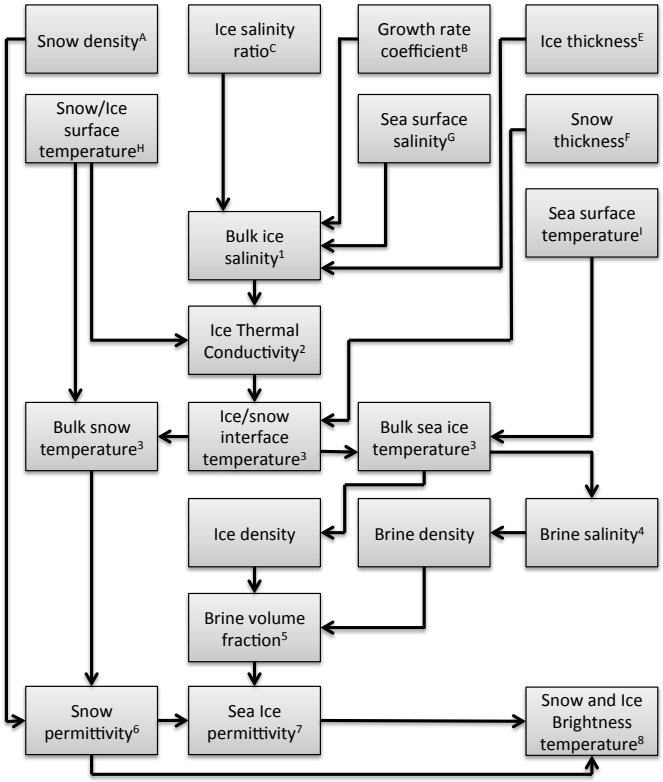

Figure 1. Simplified schematic illustration for the determination of auxiliary parameters provided to the radiative transfer models utilized in this study. The studies for the methods are listed in Table 1. A listing of all input data and the most important parameters is given in Table 2. Boxes with white background indicate input data from OPAP5 reanalyses.

Table 1. Applied methods to obtain auxiliary parameters for brightness temperatures calculations above sea ice and snow. The numbers in the first row refer to the numbers in Fig.1.

No.	Parameter	References
1	Bulk ice salinity	Ryvlin (1974)
2	Ice thermal conductivity	Untersteiner (1964)
3	Snow/Ice interface and bulk temperatures	Maykut and Untersteiner (1971)
4	Brine salinity	Vant et al. (1978); Leppäranta and Manninen (1988)
5	Brine volume fraction	Cox and Weeks (1983)
6	Snow permittivity	Tiuri (1984)
7	Sea ice permittivity	Vant et al. (1978)
8	Brightness temperatures	Kaleschke et al. (2010), Maaß et al. (2013)

The Cryosphere Discuss., doi:10.5194/tc-2016-273, 2016
Manuscript under review for journal The Cryosphere
Published: 5 December 2016

Sea water emissivity calculations are based on Fresnel equations with the descriptions of sea water after Ulaby et al. (1981) with permittivities obtained by Klein and Swift (1977). Wind induced sea surface roughness influences are assumed to be small and will be neglected (Dinnat et al., 2003). To account for corrections of the galactic background radiation and atmospheric deviations a simplified atmospheric model (Peng et al., 2013) is taken forced by climatological data from 65 years of NCEP data (Kalnay and Kanamitsu, 1996). The cosmic contribution to the overall brightness temperatures is set to 2.7 Kelvin. In these simulations, we restrict the brightness temperature calculation to nadir incidence angle. The freezing temperature of sea water is set to -1.8°C.

The single-layer model

Individual modifications of the coherent radiative transfer model of Kaleschke et al. (2010) as used in Tian-Kunze et al. (2014) include the assumption of a dielectric slab of sea ice with a semi- infinite layer of air on top and a semi-infinite layer of ocean water below (the model is further referred to as KA2010). The model considers a single layer of bare sea ice. To obtain an incoherent solution, Kaleschke et al. (2010) extends the model with a sea ice roughness approximation. As long as the root mean square thickness variations of the illuminated footprint are much larger than the electromagnetic wavelength used in the model, it is possible to average the emissivity over a variety of sea ice thicknesses which assumes all coherent propagation effects are averaged out. The model does not add a separate snow layer on top of the sea ice (thermal conductivity set to climatological value of $k_{snow} = 0.31$ (Yu and Rothrock, 1996)). In that setup, snow influences the brightness temperatures by a temperature insulation of sea ice from the atmosphere. As snow covers the ice it dampens the influence of atmospheric temperature changes to the ice. The effect appears to be significant and can be considered within the sea ice/snow interface temperature. An additional thermodynamic model as used in Tian-Kunze et al. (2014) becomes redundant since we use auxiliary data for surface temperatures.

The multi-layer model

The incoherent model used in Maaß et al. (2013) is based on radiative transfer equations and describes the emitted radiation from a stratified bare soil (referred as MA2013). The core equations are taken from Burke et al. (1979), but it has been substantially modified to suit the needs for sea ice. In our simulations the MA2013 model consists of three layers of sea ice and one layer of snow on top of the ice. All ice layers have the same properties except for the sea ice thickness that is simply divided by the number of layers considered and the ice temperature that linearly changes between the lowest layer bordering the ocean and the upper layer facing the atmosphere. The snow is assumed to be dry and has a snow density of $\rho_{snow} = 330\ [kg/m^3]$. In contrast to the previous model, the snow layer does not only affect the temperature of the underlying sea ice, but also the radiation incidence angle, potentially leading to propagation effects. Snow changes the refraction index and thus the reflectivity between the air-snow and snow-ice boundaries. By changing the optical properties of the air-ice boundary and the temperature of sea ice, snow has a passive effect on the brightness temperature (Schwank Mike et al., 2015).

As an addition to the model described in Maaß et al. (2013) we added the ability to take multiple reflections and refractions within the sea ice into account. Thus, the radiative beams are followed on their way through the layers of snow and ice and

The Cryosphere Discuss., doi:10.5194/tc-2016-273, 2016
Manuscript under review for journal The Cryosphere
Published: 5 December 2016

Table 2. Input parameters provided for the calculation scheme. The letters refer to Fig. 1.

Letter	Input parameter	Value	References / Source
A	Snow density	330 [kgm^{-3}]	
B	Thermal conductivity of snow	0.31 [Wm^{-1}K^{-1}]	Yu and Rothrock (1996)
C	Ice salinity ratio	0.175	Kovacs (1996)
D	Growth rate coefficient	0.5	Ryvlin (1974)
E	Sea ice thickness	variable	ORAP5
F	Snow thickness	variable	ORAP5
G	Sea surface salinity	variable	ORAP5
H	Snow/ice surface temperature	variable	ORAP5
I	Sea surface temperature	variable	ORAP5
H	Sea ice concentration	variable	ORAP5

added up when they leave the medium in upper direction towards the atmosphere. Reflected beams are removed after 15 interface passings when they are not able to leave the ice-snow medium on the short term. At this point, the intensity of the radiative beams are negligible and we are able to cap the computational effort for the calculation.

2.1 The ORAP5 reanalyses

The radiative transfer models are forced using data from the Ocean ReAnalysis Pilot 5 (ORAP5) project, which is provided by the European Centre of Medium range Weather Forecast (ECMWF) (Tietsche et al., 2014). The sea ice and snow thicknesses, the surface and sea water temperatures, the sea ice fractional coverage and the sea surface salinity are taken from ORAP5 data (Table 2). The NEMO global ocean model version 3.4 has been utilized to run on the DRAKKER ORCA025.L75 configuration for 34 years, covering the years from 1979 to 2013. The configuration uses a tripolar mesh grid with poles located in Greenland and Central Asia in the northern hemisphere, as well as a pole in the Antarctic in the southern hemisphere. The spatial resolution ranges from 1/4 degree at the equator to a couple of kilometers in the polar regions with 75 vertical levels in the ocean.

The dynamic-thermodynamic Louvain-la-Neuve Sea Ice Model second generation (LIM2) has been coupled to the NEMO ocean model (Bouillon et al., 2009). Sea ice is represented with a two-dimensional viscous-plastic rheology that interacts with the atmosphere and the ocean. A simple three-layer model (one for snow and two layers for ice) is used at which sensible heat storage and vertical heat conduction are determined. Vertical heat fluxes are calculated based on the thermodynamic energy balance according to Semtner (1976). The albedo is a function of the snow and ice thicknesses, the state of the surface and the cloudiness. Sea ice coverage is taken from the Operational SST and Sea Ice Analysis (OSTIA) system, which assimilates sea ice concentration from the Satellite Application Facility on Ocean and Sea Ice (OSI-SAF) dataset produced by the European Organization for the Exploitation of Meteorological Satellites (EUMETSAT).

This study focuses on the winter season in 2012/2013, more precisely on November in 2012 and March 2013. The period has been chosen due the availability of the reanalyses dataset ORAP5 and SMOS measurements (v. 5.05). As a pilot-project

The Cryosphere Discuss., doi:10.5194/tc-2016-273, 2016
Manuscript under review for journal The Cryosphere
Published: 5 December 2016

with the goal to deliver ocean reanalyses with highest quality standards the dataset is not yet operational and therefore further processed. The second limiting factor is a reasonable time-frame to describe brightness temperature changes with varying sea ice thicknesses. In the melting season, when melt ponds form on sea ice and temperatures begin to rise, SMOS brightness temperatures over sea ice are impossible to connect to a specific sea ice property (Kaleschke et al., 2010). Thus, November and March are the first and the last month, respectively, with full monthly data coverage from SMOS and therefore chosen.

2.2 SMOS brightness temperatures

SMOS is equipped with a passive microwave 2D-interferometer called MIRAS (Microwave Imaging Radiometer with Aperture Synthesis) operating in L-Band at 1.4 GHz (~21 cm). It measures brightness temperatures in full-polarization up to 65° incidence angle every 1.2 seconds (Kerr et al., 2001). The hexagonal snapshots have a swath-width of around 1200 km, which allows a global coverage. Each point on earth is observed at least once every three days with a daily coverage in the polar regions due to SMOS quasi-circular sun-synchronous orbit at 758 km height.

SMOS snapshots are influenced by Radio frequency interference (RFI) rooting from radar, TV and radio transmission (Mecklenburg et al., 2012). To account for the most critical disturbances, a RFI filter has been utilized. Brightness temperatures above 300 K identify a snapshot to be RFI-contaminated and be further ignored for the brightness temperature product. The threshold of 300 K is chosen as values higher than that are not expected to be seen in the Arctic or Antarctic.

The brightness temperature product consists of vertical and horizontal polarization, which are averaged up to 40° incidence angle when they are taken within 2.5 seconds time-interval (Kaleschke et al., 2012). These brightness temperatures are said to represent L-Band measurements at nadir as brightness temperature changes that are connected to the varying incidence angles are expected to cancel out each other when both polarisations are considered. The averaged product is available on a daily basis up to 85° latitude. The data is collected for an entire day and is averaged for each grid point to provide a L3B daily mean brightness temperature product. Finally, the data is geolocated on a NSIDC polar-stereographic projection that provides grid cells with the same areal extent of 12.5 km horizontal resolution.

3 Sea water correction

To investigate the quality of the radiative transfer models for partially covered sea ice areas in the ORAP5 setup, we first check the representation of emissivities over open ocean of the models. As mentioned before, both models use the same equations to calculate the emissivity of water areas based on Klein and Swift (1977) and will thus produce the same brightness temperatures using same input data. Therefore we here only show the correction for MA2013. In any case, L-Band brightness temperature variations in open Arctic waters are low compared to sea ice and should fairly match between observed SMOS and simulated brightness temperatures from the radiative transfer models (Berger et al., 2002).

We simulate brightness temperatures in all open water areas north of 50° latitude. As a first step, we project the ORAP5 reanalyses on the polar-stereographic grid SMOS is using. Afterwards, we obtain a monthly average by calculating brightness temperatures for each day of the month using daily input data. Then, we average all brightness temperatures corresponding to

The Cryosphere Discuss., doi:10.5194/tc-2016-273, 2016
Manuscript under review for journal The Cryosphere
Published: 5 December 2016

a single day to a monthly value. We find an average bias of 3.093 Kelvin between MA2013 and the SMOS observations in November and March (Fig. 2). To identify the open water areas, we exclude all data points with potential sea ice on it and also exclude all data points flagged as land. Furthermore, brightness temperatures of more than 120 Kelvins are most unlikely to account for Arctic open water areas and are excluded as well. Finally, a total of 99085 data points show an average open water brightness temperature of SMOS $\overline{TB}_{SMOS} = 100.68K$, whereas the models have an average of $\overline{TB}_{model} = 97.58K$.

To correct for the bias of open water areas we add the difference of 3.093 Kelvin to the overall brightness temperature of sea water. Subsequent results of the radiative transfer models show the main accumulation of data points at around 100 Kelvins and a second, weaker one beginning at 105, each one with a tail towards higher brightness temperatures of SMOS. The first tail at 100 Kelvin can be explained by the gradual transition between land and water areas. As the SMOS land product only distinguishes between fully covered land and water points, it does not represent partially covered measurements of pixels containing land and water. The region of higher TBs are located in the Baltic Sea. In that area, lower sea surface salinities and higher water temperatures compared to the rest of the Arctic waters leads to higher brightness temperatures. The water bias correction is used in all following simulations using the radiative transfer models.

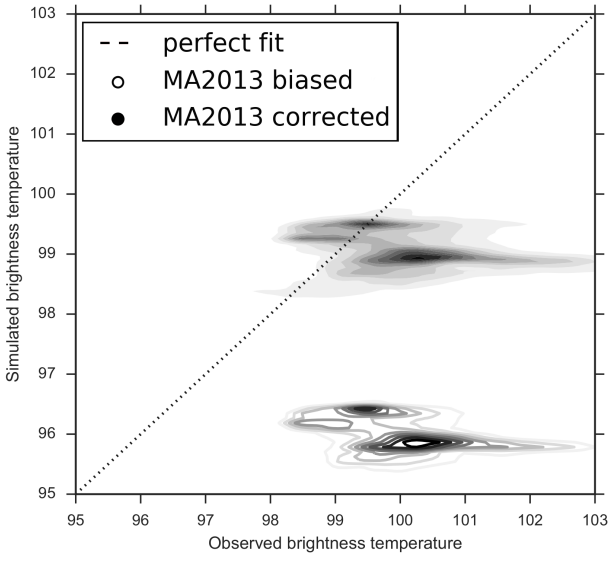

Figure 2. Open water brightness temperature comparison between SMOS and MA2013. A water bias correction is applied to all simulated brightness temperatures.

4 Brightness temperature comparison

Brightness temperatures simulated with MA2013 are generally higher than brightness temperatures of KA2010 up to around 15 Kelvins (Fig. 3). Largest differences are located in the outer sea ice zones with highest magnitude where sea ice concentrations

The Cryosphere Discuss., doi:10.5194/tc-2016-273, 2016
Manuscript under review for journal The Cryosphere
Published: 5 December 2016

are close to 100%, and an increase of sea ice thickness is expected, such as in the East Siberian Sea or the Canadian Arctic Archipelago in November. For a first evaluation of the brightness temperature models, the two extreme cases of open water and 100% multi-year thick sea ice can be considered. Since we already treated the lower boundary of open ocean brightness temperatures with a water bias correction as indicated above, we now concentrate on the upper boundary of a saturated signal over thick sea ice areas. We find higher brightness temperatures in the central parts of the Arctic simulated by MA2013. The saturated value in MA2013 appears to be around ∼250 Kelvin whereas KA2010 only shows ∼240 Kelvins. The differences between both models are lowest in the areas where multi-year sea ice is expected close to Greenland (NSDIC). There is no indication for seasonal changes between brightness temperatures from November and March expect the increased area covered by sea ice. The variability in November shows a slightly larger spatial variation of brightness temperature due to more new sea ice formation.

Brightness temperatures measured by SMOS appear to be in between the simulated ones of KA2010 and MA2013 influenced by strong spatial differences (Fig. 4). In November 2012, both models show higher brightness temperatures in the East Siberian Sea and the Canadian Arctic Archipelago. Lower brightness temperatures are located in the Canadian Basin and the Chukchi Sea with extension to the Bering Street. A different picture is shown in the central Arctic at grid points with more than 80% sea ice concentration coverage, where both models simulate brightness with deviations to opposite directions. The model of KA2010 shows lower (-2.84 ± 5.58K) and MA2013 higher (9.17 ± 5.69K) brightness temperatures compared to SMOS observations. The same is true for March 2013, although that KA2010 (0.39 ± 4.04K) shows a stronger agreement in the central Arctic than MA2013 (10.78 ± 4.31K). In November 2012, brightness temperature deviations between KA2010 and the SMOS measurements are of smaller spatial extent than in MA2013 and show a higher variability between positive and negative differences. MA2013 appears to be positively biased not only in November 2012, but also in March 2013. The simulations exceed SMOS brightness temperatures almost everywhere in the Arctic with deviations up to 20 Kelvins in the Labrador Sea and Sea of Okhotsk. There are no large differences observed in open water areas, except places close to coastal areas that confirms the quality of the water bias correction .

A general comparison between all simulated and modeled brightness temperatures in the Arctic show that most data points are located in the open water region at around 105 Kelvins and more central areas at around 240 Kelvins (Fig. 5). The latter is associated with thicker sea ice related to saturated brightness temperatures at 1.4 GHz. In November, simulated brightness temperature appear to correspond with SMOS measurements. KA2010 shows lower brightness temperatures of around 2 Kelvins throughout the whole range, whereas MA2013 simulates larger brightness temperatures in thick ice regions. Furthermore, as already seen in figure 4, MA2013 overestimates brightness temperatures above ∼190 Kelvins also in March. The individual brightness temperature spread is biggest in between the main clusters (not shown here), although most points appear to concentrate around the 1:1 line. The correlations of all distributions state $r = 0.98$ is astonishing, although the reason might be the overwhelming majority of points located at the open water and saturated fix points.

Figure 6 shows the cumulative probability function over all simulated and observed brightness temperatures over sea ice in the Arctic. In November approximately 40% of brightness temperatures are below 220 Kelvin, when it is only ∼ 15% in March. First, the brightness temperature distribution increases linearly until the aforementioned threshold and then quickly saturates

The Cryosphere Discuss., doi:10.5194/tc-2016-273, 2016
Manuscript under review for journal The Cryosphere
Published: 5 December 2016

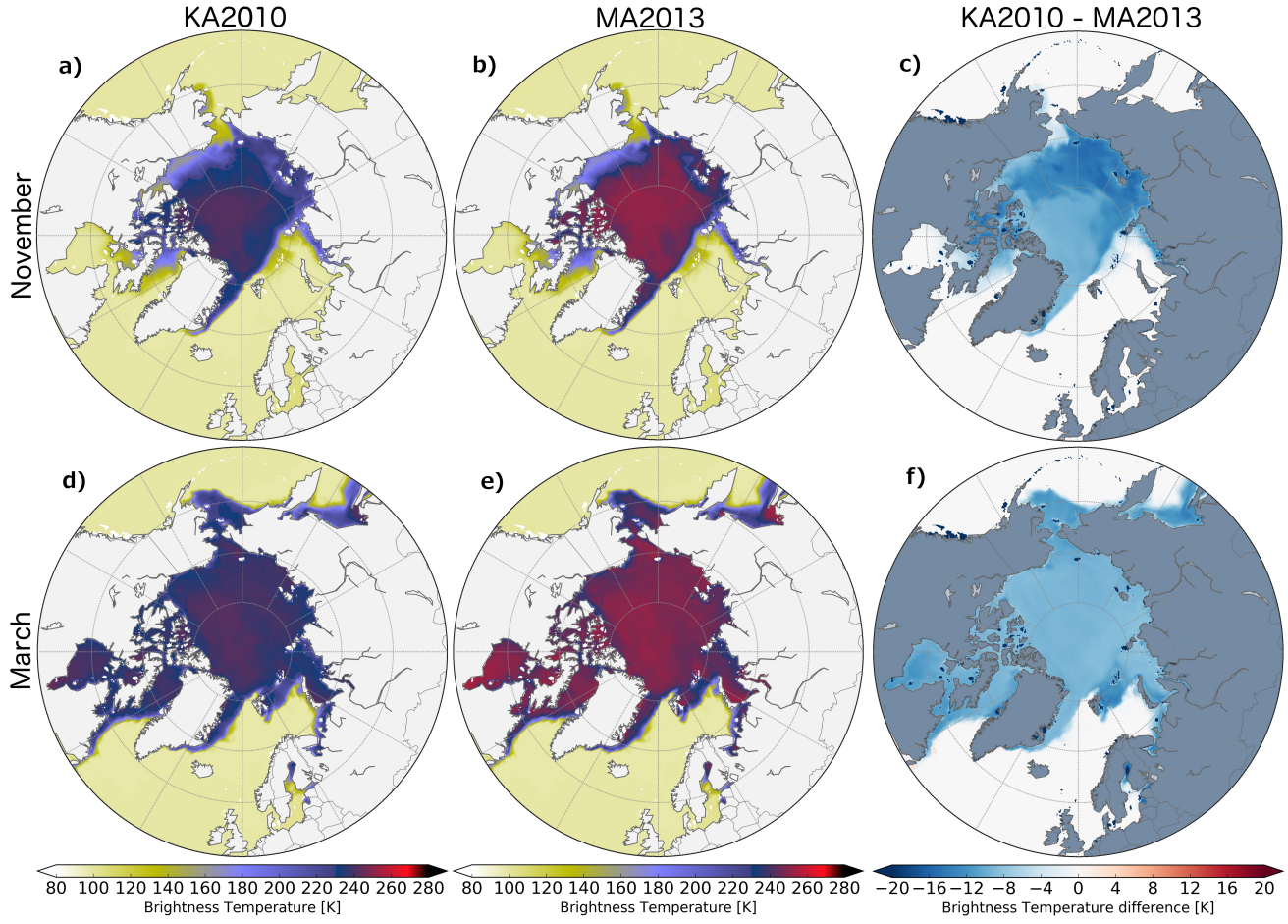

Figure 3. Monthly brightness temperatures simulated by KA2010 (left column) and MA2013 (center column). (**a-c**) shows the November 2012 brightness temperature distribution based on ORAP5 reanalyses input data with a comparison plot of both models at (**c**). (**d-f**) is equal, but for March 2013.

around 240 Kelvins. A Kolmogorov-Smirnov-Test ($\alpha = 0.1$) of the cumulative probability function over all data points of the Arctic rejects all simulated brightness temperature distributions except for KA2010 in March 2013.

5 Radiative transfer model sensitivity study

In order to identify the most important input variables for the radiative transfer models, we evaluate the sensitivity of the models to certain changes of sea ice, snow and sea water parameters. We keep all but one parameter fixed at a monthly value and calculate the brightness temperatures for the minimum and the maximum simulated value within the month for one physical parameter. That will give us two different brightness temperatures, one for the minimum, one for the maximum, of which the

The Cryosphere Discuss., doi:10.5194/tc-2016-273, 2016
Manuscript under review for journal The Cryosphere
Published: 5 December 2016

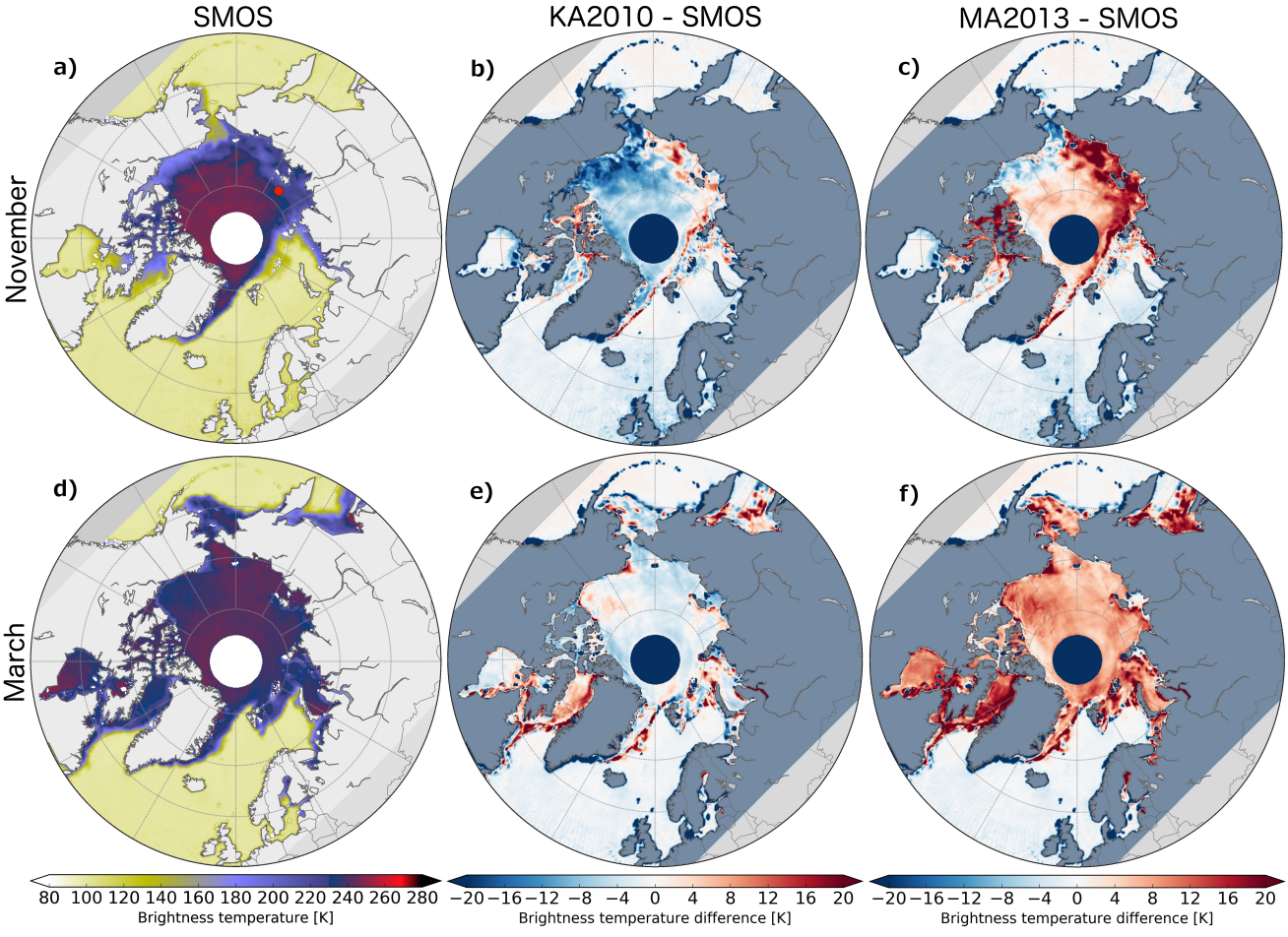

Figure 4. SMOS brightness temperatures (**a,d**) compared with simulated brightness temperatures using KA2010 (**b,e**) and MA2013 (**c,f**) in November 2012 (**a-c**) and March 2013 (**d-f**). The red dot in (**a**) indicates the position of the investigated grid cell in the Laptev Sea.

difference is the range of brightness temperature change related to one of the parameters that can be expected. Varying all input parameters provided by the ORAP5 reanalyses we quantify the impact of certain physical parameters on our brightness temperatures at a specific place over the time span of one month.

The most important input parameters for brightness temperature calculations with the radiative transfer models are the sea ice fractional coverage, sea ice thickness and sea ice temperature (Fig. 7, accounting for 92% grid points in March and November). For both seasons, the sea ice temperature has the largest impact on the brightness temperatures in the central Arctic with the largest spatial extent in MA2013. The sea ice temperature becomes even more important in March when the overall sea ice extent is greatest throughout the year in up to 25% of the Arctic. Closer to the outer sea ice regions, the sea ice fractional coverage is most influential for the largest part of the Arctic sea ice (around 60% of the total sea ice area). During

The Cryosphere Discuss., doi:10.5194/tc-2016-273, 2016
Manuscript under review for journal The Cryosphere
Published: 5 December 2016

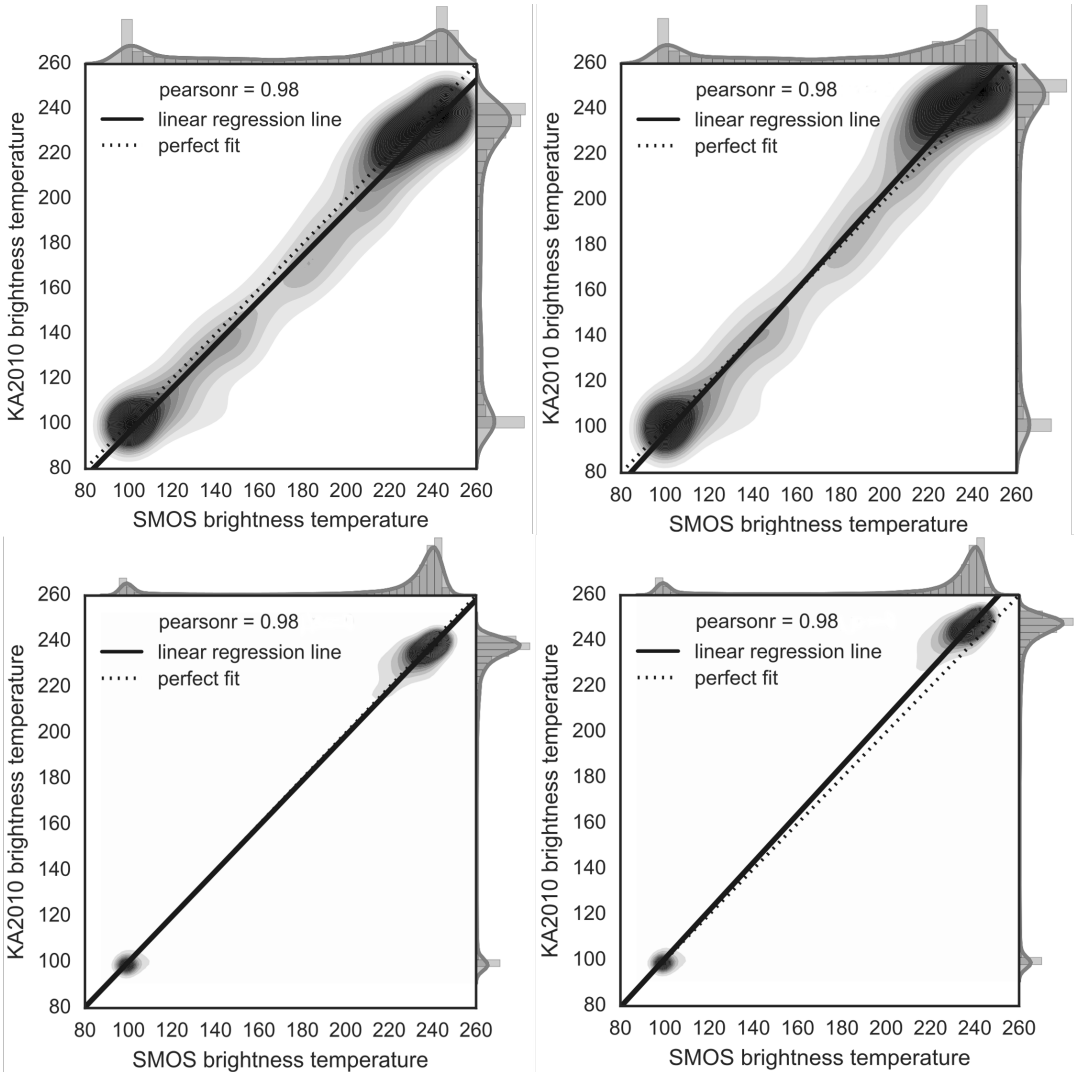

Figure 5. Brightness temperature comparison between simulated and observed brightness temperatures in November 2012 (top) and March 2013 (bottom) for KA2010 (left) and MA2013(right). The pearson correlation r between simulated and observed brightness temperatures over sea ice for MA2013 and KA2010, respectively is stated in the legend.

the sea ice growth season in November, the leading impact of sea ice fraction extends all the way to the coastal areas in the East Siberian Sea, whereas the Canadian Basin is dominated by sea ice thickness growth. In any case, the sea ice thickness is most important in a large area close to the sea ice edge (25% of the area in November). This is partially true when sea ice thicknesses are predominantly thicker than half a meter and exceed SMOS sensitivity (5% in March). However, the effect of sea ice concentration and thickness is similar in both models. In the very outer marginal sea ice zone it appears that sea surface

The Cryosphere Discuss., doi:10.5194/tc-2016-273, 2016
Manuscript under review for journal The Cryosphere
Published: 5 December 2016

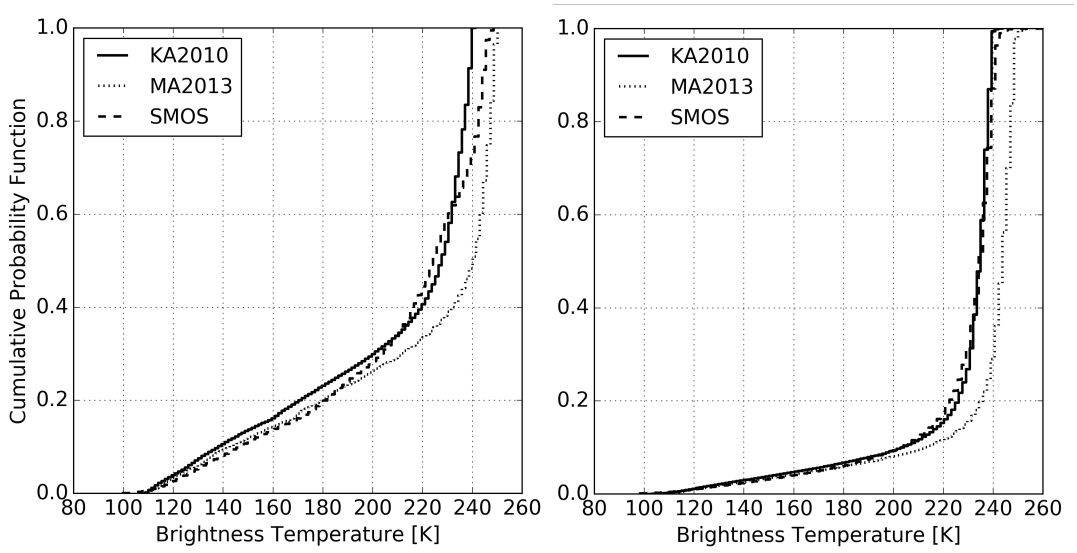

Figure 6. Cumulative probability density function of Arctic-wide brightness temperatures over sea ice in November 2012 (left) and March 2013 (right).

temperature dominates (7%). The sea surface salinity only contributes in very small areas in the Fram-Strait where sea surface temperatures and salinities are higher (<1%).

For a more detailed analysis on the contribution of sea ice thickness and concentration to the modelled brightness temperatures, a sample freeze-up situation is investigated at a point located in the Laptev Sea (77.5°N, 137.5°E) from October to November 2012 (Fig. 8). The observational sea ice concentration product ASI (ARTIST Sea Ice algorithm, (Kaleschke et al., 2001; Spreen et al., 2008) shows a rapid freeze-up to 80% sea ice coverage in just a few days. The brightness temperatures of SMOS measurements and the KA2010 and MA2013 models properly agree with some exceptions on the first days of the freezing period that starts around the 25. October. The simulated brightness temperatures appear to be underestimated at the beginning of the season which leads to a more linear brightness temperature increase rather than a logarithmic shape as observed from the SMOS measurements. However, the simulated sea ice concentration of ORAP5 appears to be lower than the the observed ASI sea ice concentration and needs almost two weeks to catch up to the same coverage as ASI. The sea ice thickness on the other hand shows a fast thickening to more than half a meter even before the main freeze-up event takes place. The sea ice growth model of Lebedev (1938) accumulates sea ice as a function of the temperature difference between the surface air temperatures and freezing point of water, as well as the number of freezing days below zero degrees. In contrast to the sea ice thickness of ORAP5, Lebedevs' parameterization shows a gradual increase of ice thickness throughout the freeze-up event. Following, we observe an underestimation of sea ice concentration and an overestimation of sea ice thicknesses, although the brightness temperatures between observational and simulated data fits decently well.

The Cryosphere Discuss., doi:10.5194/tc-2016-273, 2016
Manuscript under review for journal The Cryosphere
Published: 5 December 2016

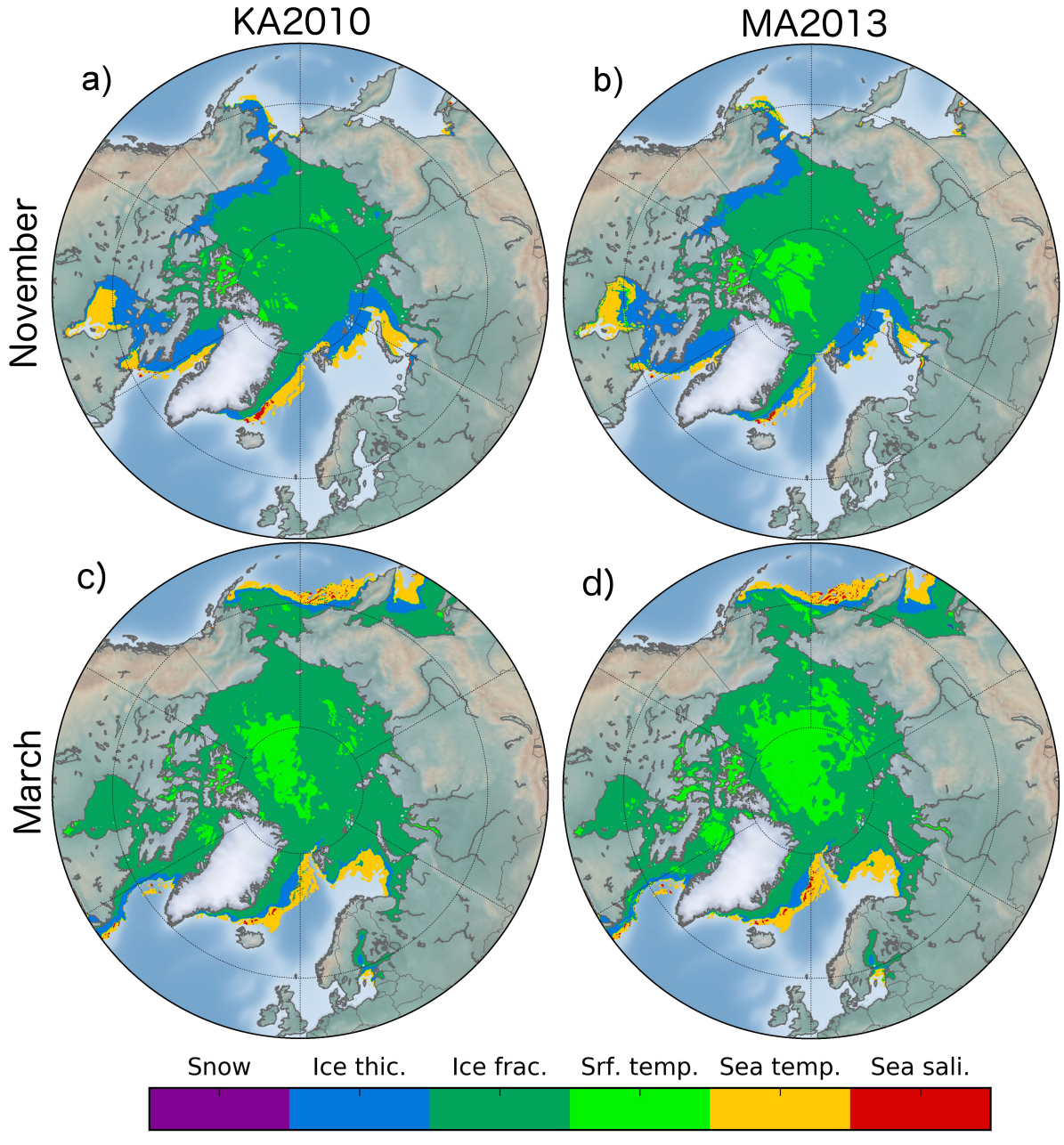

Figure 7. Most influencial physical variables from ORAP5 on the brightness temperature gradient. Monthly values are shown for November 2012 (**a-b**) and March 2013 (**c-d**) for KA2010 (**a-c**) and MA2012 (**b-d**).

The Cryosphere Discuss., doi:10.5194/tc-2016-273, 2016
Manuscript under review for journal The Cryosphere
Published: 5 December 2016

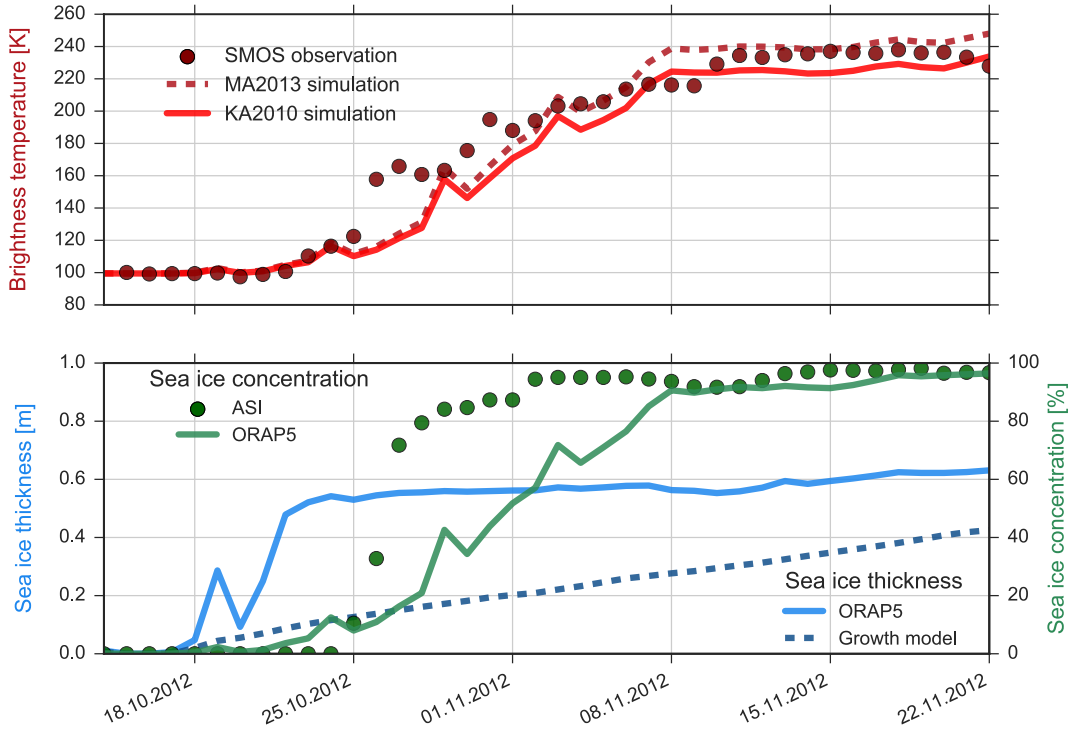

Figure 8. Freeze-up event in October to November 2012 that took place in the Laptev Sea (77.5 N, 137.5 E). Brightness temperature time-series of from KA2010, MA2013 and SMOS measurements (top) and sea ice thickness and concentration time-series of ORAP5, ASI and Lebedev retrieval model data (bottom).

6 Discussion

The simulated brightness temperatures from two incoherent radiative transfer models with ORAP5 input data generally match the SMOS observations in an overall Arctic-wide comparison. The analysis shows spatial differences throughout the Arctic with largest differences in the outer Arctic regions for November 2012 and March 2013. However, the sign of the deviation changes according to the region. In the East Siberian Sea both models simulate higher brightness temperatures compared with SMOS, whereas lower values are shown in the Canadian Basin. In the latter the fractional sea ice coverage increased up to an average value of 60% in November, whereas the coverage in the East Siberian Sea kept more or less constant at 100% (not shown here). The Canadian Basin experienced an initial freeze-up from open ocean to a thin sea ice layer. As microwave radiation in L-Band is most sensitive to changing sea ice with thicknesses of only a few centimeters (e.g. Kaleschke et al. (2012)), sea ice concentration changes become more important the thicker the sea ice gets and brightness temperatures approach saturation. That makes it necessary to use a high-precision auxiliary sea ice concentration product to account for brightness temperature changes due to alteration in sea ice concentration. As we provide sea ice fractional coverage from our reanalyses to the radiative transfer models, we are able to reduce the uncertainty of sea ice fraction changes compared to studies

The Cryosphere Discuss., doi:10.5194/tc-2016-273, 2016
Manuscript under review for journal The Cryosphere
Published: 5 December 2016

with an assumption of a constant 100% sea ice concentration coverage (Tian-Kunze et al., 2014). However, changes still remain essential. An uncertainty of 10% fractional sea ice coverage accounts for a difference of 15 Kelvins at sea ice thicknesses of around 40 cm (Kaleschke et al., 2010). In the same scenario, a brightness temperature change of 15 Kelvins may stand for a sea ice thickness uncertainty of more than 20 cm.

In order to assimilate thin sea ice thicknesses it is crucial to understand the impact of all physical parameters on the brightness temperature simulations. Kaleschke et al. (2012) found sea ice concentration and thickness changes in thin sea ice areas are the most important variables for L-Band brightness temperatures. We here support this evidence as the dominating dependencies for brightness temperature simulations are found to be the same throughout the Arctic (Fig. 7). Over thick sea ice in the central Arctic we find the sea ice/snow surface temperature to be the most influential parameter. Since sea ice concentration is close to 100% and sea ice thicknesses are above L-Band sensitivies, brightness temperature changes are due to the impact of snow and sea ice/snow temperature changes that comes with it. Our results also show a significant influence of sea ice/snow and sea surface temperatures in areas of thin sea ice close to the ice edge. This is explained by a fractional sea ice coverage of less than 10%, where brightness temperature variations are dominated by changing open water emissivities. We point out that sea surface temperature and salinities get more important in regions with lower sea ice coverage. Therefore, in case partially covered sea ice concentrations are taken into account we caution that a climatology of sea ice/snow surface temperatures or sea surface salinities might not be sufficient enough to picture the transition between open water towards the sea ice edge. This is especially true for the declining sea ice observed in the recent years as the sea ice edge is likely to be located at a different location than in the previous years.

Our results indicate that brightness temperature differences up to around 15 Kelvin can be due to the usage of different radiative transfer models (Fig. 3). Even though both models tend to have the same signatures, KA2010 shows lower brightness temperatures than the MA2013 in the whole Arctic. This was expected as the MA2013 model is able to take multiple sea ice layers into account, as well as the radiometric effect of snow on top of sea ice, whereas KA2010 only indirectly includes the effect of snow with the representation of the thermodynamic insulation effect. Compared with SMOS brightness temperatures, it appears that MA2013 overestimates brightness temperatures in many parts of the Arctic, most pronouncedly in March in the central Arctic region. For a brightness temperature assimilation this would be rather detrimental, as we only expect benefits from SMOS-based ice thickness assimilation thin sea ice regions because microwave radiation is not able to distinguish between thicker sea ice. In contrast, KA2010 shows good agreement in the central Arctic area. For brightness temperature assimilation purposes that would be clearly beneficial as the main assimilation should take place in regions with thin sea ice rather than in the central Arctic. Additionally, MA2013 shows a rapid brightness temperature rise in the transition from open water towards the very first centimeters of sea ice (Kaleschke et al. (2010), Maaß et al. (2013)). Therefore, a more comprehensive representation of sea ice with radiative transfer equations using a multiple layers does not necessarily need to be an advantage for brightness temperature assimilation.

The majority of all data points accumulates in the vicinity of the perfect fit, although in March, most of the data points are located at brightness temperatures for either the saturated case at 240/250 Kelvin for KA2010/MA2013 or open water areas (Fig. 5 and Fig. 6). The overall performance in terms of the range of simulated brightness temperatures over sea ice is explained

The Cryosphere Discuss., doi:10.5194/tc-2016-273, 2016
Manuscript under review for journal The Cryosphere
Published: 5 December 2016

by the Kolmogorov-Smirnov test. The test accepts only the brightness temperature distribution from March 2013 of KA2010. The reason is because 92% of all simulated data points are higher than 220 Kelvin. Therefore, it is most important for the model to agree with the saturated case in order to determine reasonable areas for brightness temperature assimilation. Thus, based on ORAP5 reanalyses input data and electromagnetic formulations used here, we suggest to use the KA2010 radiative transfer model for brightness temperature assimilation. Note, that this is no statement about the quality of the radiation model in general, than rather a suggestion for the specific specification utilized in this study in terms of applied assumptions and characteristics of the LIM2 sea ice model.

Although the statistical representation of brightness temperatures is well captured we find large discrepancies in times of rapid sea ice changes (Fig. 8). ORAP5 appears to have difficulties to simulate freeze-up events by both, an overestimation of sea ice thickness and an underestimation of sea ice concentration. The assimilation of OSI-SAF sea ice concentration into ORAP5 pushes the sea ice concentration into the right direction, but appears to be too slow to picture changes in a short period of time. A smaller fractional sea ice concentration and an overestimation of sea ice thickness then leads to simulated brightness temperatures that fit with observed SMOS brightness temperatures, even though both parameters are clearly wrong at this time. In this case, a SMOS brightness temperature assimilation in ORAP5 may not bring much benefit as we cannot distinguish between the influence of sea ice concentration and thickness. An auxiliary sea ice concentration data product is needed to correct brightness temperature calculations for possible differences in sea ice cover. We therefore suggest a combined assimilation of brightness temperatures covering a broad spectral range from 1.4 to 37 GHz yielding information on both, sea ice thickness and concentration.

All brightness temperature calculations rely on the quality of the ORAP5 data as the results are highly influenced by uncertainties of the input parameters. A comprehensive sea ice concentration and sea ice thickness comparison between ORAP5 and observational products was made by Tietsche et al. (2015) who found an agreement of sea ice concentration in ORAP5 and OSTIA in the order of magnitude of 5% root mean square deviation. As aforementioned, this uncertainty accounts for 7-8 Kelvin, explaining up to more than 10 cm ice thickness difference in case of thicker sea ice and is therefore still critical. They point out that thin sea ice regions need further improvements, especially in the vicinity of the ice edge. However, the initial freeze-up sea ice thickness in the LIM2 sea ice model is set to 0.5 m leading to an overestimation of sea ice thicknesses in newly formed sea ice areas. Sea ice of half a meter thickness is already at the maximum thickness for a brightness temperature assimilation and will lead to essential brightness temperature differences between modeled and observational data. This is a strong argument for a brightness temperature assimilation, as it might help to correct the overestimation of ORAP5 sea ice thicknesses in freeze-up areas.

7 Summary and outlook

The radiative transfer models from Kaleschke et al. (2010) (denoted as KA2010) and Maaß et al. (2013) (MA2013) are taken as a forward operator to simulate brightness temperatures at 1.4 GHz in the winter season 2012/2013 and to identify the feasibility of the models for a brightness temperature assimilation in the global ocean reanalyses product ORAP5. Using ORAP5 input

The Cryosphere Discuss., doi:10.5194/tc-2016-273, 2016
Manuscript under review for journal The Cryosphere
Published: 5 December 2016

data, we compared modeled brightness temperatures with SMOS observations in November 2012 and March 2013 accounting for the start and the end of the winter season, respectively.

The results of this study indicate that both models are able to simulate Arctic-wide monthly brightness temperatures. We are able to observe a similar increase of simulated and observed brightness temperatures from thin to thicker sea ice areas. Although both models show a decent fit in November, the model of Maaß et al. (2013) tends to overestimate brightness temperatures in the saturated case of thick sea ice in March with the configurations applied here. A Kolmogorov-Smirnov test thus only accepts the brightness temperature distribution of KA2010 in March by taking the SMOS observation as the reference probability distribution. All other, especially the results of MA2013 in March, are rejected. Therefore, we suggest to use the model of KA2010 for a brightness temperature assimilation into the ORAP5 reanalyses project.

The most important parameters for the brightness temperature calculations over thin sea ice are identified to be the sea ice thickness and sea ice coverage. This result supports the findings of other studies (e.g. Kaleschke et al. (2012)). In thicker sea ice areas the dominant parameter is the sea surface temperature since the sea ice fractional coverage is close to 100% and sea ice thickness changes do not affect the measurements at 1.4 GHz. However, the smaller the sea ice fractional coverage, the more important are the sea surface temperature and salinity. This becomes relevant at sea ice concentrations below 15%, usually in small regions at the very outer sea ice edge.

The brightness temperature assimilation is expected to result in more accurate sea ice thicknesses analysis than a direct assimilation of the physical parameter as the climate model provides a series of input variables to the forward operator. These variables do not need to be replaced by climatologies, parameterizations or assumptions that may inflict the results of our sea ice thickness retrieval. However, even though the sea ice thickness and concentration in ORAP5 are well constrained by observations (Tietsche et al., 2015), both show difficulties to represent a rapid freeze-up event with an underestimation of sea ice concentration and an overestimation of sea ice thickness. That reveals the challenge to use brightness temperatures to correct for the right physical parameter and magnitude. We recommend to combine the brightness temperature assimilation for sea ice thickness with the assimilation of an independent auxiliary observational sea ice concentration product or the simultaneous assimilation of measurements taken at higher microwave frequencies, e.g. up to 37 GHz.

The assimilation of SMOS brightness temperatures appears to be a great chance for a better representation of sea ice thicknesses in the ORAP5 reanalyses. Substantial differences between observational and simulated brightness temperatures are found to be largest in regions with thin sea ice, in which SMOS uncertainties of the sea ice thickness retrievals are lowest (Kaleschke et al., 2010). That reveals the possibility to retrieve and correct sea ice thicknesses in future investigations. However, to what magnitude these results translate to other reanalyses products or climate forecasts has to be investigated.

8 Data availability

L3B Brightness temperatures are provided by the CliSAP-Integrated Climate Data Center (ICDC) on http://icdc.cen.uni-hamburg.de/1/daten/cryosphere/l3b-smos-tb.html (Tian-Kunze et al., 2012). The reanalyses data of ORAP5 was kindly provided by

The Cryosphere Discuss., doi:10.5194/tc-2016-273, 2016
Manuscript under review for journal The Cryosphere
Published: 5 December 2016

the ECMWF and is freely available on http://marine.copernicus.eu/services-portfolio/access-to-products/?option=com_csw&view=details&product_id=GLOBAL_REANALYSIS_PHYS_001_017 (Zuo et al., 2015).

Acknowledgements. We thank Steffen Tietsche for the provision of high-quality ORAP5 reanalyses data, Andreas Wernecke who helped to implement the cosmic and galactic background radiation representation. We thank the "Science Snack" team for fruitful discussions.

References

Albergel, C., Rosnay, P. D., Gruhier, C., Muñoz-sabater, J., Hasenauer, S., Isaksen, L., Kerr, Y., and Wagner, W.: Evaluation of remotely sensed and modelled soil moisture products using global ground-based in situ observations, Remote Sensing of Environment, 2011.

Berger, M., Camps, a., Font, J., Kerr, Y., Miller, J., Johannessen, J., Boutin, J., Drinkwater, M. R., Skou, N., Floury, N., Rast, M., Rebhan, H., and Attema, E.: Measuring ocean salinity with ESA's SMOS mission - Advancing the science, Esa Bulletin-European Space Agency, pp. 113–121, ISI:000178657500018, 2002.

Bouillon, S., Morales Maqueda, M. a., Legat, V., and Fichefet, T.: An elastic-viscous-plastic sea ice model formulated on Arakawa B and C grids, Ocean Modelling, 27, 174–184, doi:10.1016/j.ocemod.2009.01.004, http://dx.doi.org/10.1016/j.ocemod.2009.01.004, 2009.

Burke, W. J., Schmugge, T., and Paris, J. F.: Comparison of 2.8- and 21-cm microwave radiometer observations over soils with emission model calculations, Journal of Geophysical Research, 84, 287–294, doi:10.1029/JC084iC01p00287, 1979.

Cox, G. F. and Weeks, W. F.: Equations for determining the gas and brine volumes in sea ice samples, Tech. rep., 1983.

Dinnat, E. P., Boutin, J., Caudal, G., and Etcheto, J.: Issues concerning the sea emissivity modeling at L band for retrieving surface salinity, Radio Science, 38, n/a–n/a, doi:10.1029/2002RS002637, http://doi.wiley.com/10.1029/2002RS002637, 2003.

Kaleschke, L., Heygster, G., and Lüpkes, C.: SSM/I sea ice remote sensing for mesoscale ocean-atmosphere interaction analysis: Ice and icebergs, ... of Remote Sensing, http://cat.inist.fr/?aModele=afficheN{&}cpsidt=14060986, 2001.

Kaleschke, L., Maaß, N., Haas, C., Hendricks, S., Heygster, G., and Tonboe, R. T.: A sea-ice thickness retrieval model for 1.4 GHz radiometry and application to airborne measurements over low salinity sea-ice, Cryosphere, 4, 583–592, doi:10.5194/tc-4-583-2010, 2010.

Kaleschke, L., Tian-Kunze, X., Maaß, N., Mäkynen, M., and Drusch, M.: Sea ice thickness retrieval from SMOS brightness temperatures during the Arctic freeze-up period, Geophysical Research Letters, 39, n/a–n/a, doi:10.1029/2012GL050916, http://doi.wiley.com/10.1029/2012GL050916, 2012.

Kaleschke, L., Tian-Kunze, X., Maaß, N., Beitsch, A., Wernecke, A., Miernecki, M., Müller, G., Fock, B. H., Gierisch, A. M., Schlünzen, K. H., Pohlmann, T., Dobrynin, M., Hendricks, S., Asseng, J., Gerdes, R., Jochmann, P., Reimer, N., Holfort, J., Melsheimer, C., Heygster, G., Spreen, G., Gerland, S., King, J., Skou, N., Søbjærg, S. S., Haas, C., Richter, F., and Casal, T.: SMOS sea ice product: Operational application and validation in the Barents Sea marginal ice zone, Remote Sensing of Environment, doi:10.1016/j.rse.2016.03.009, http://linkinghub.elsevier.com/retrieve/pii/S003442571630102X, 2016.

Kalnay, E. and Kanamitsu, M.: The NCEP/NCAR 40-Year Reanalysis project, Bulletin of the ..., http://journals.ametsoc.org/doi/abs/10.1175/1520-0477(1996)077{%}3C0437:TNYRP{%}3E2.0.CO;2, 1996.

Kerr, Y. H., Waldteufel, P., Wigneron, J. P., Martinuzzi, J. M., Font, J., and Berger, M.: Soil moisture retrieval from space: The Soil Moisture and Ocean Salinity (SMOS) mission, IEEE Transactions on Geoscience and Remote Sensing, 39, 1729–1735, doi:10.1109/36.942551, 2001.

Kerr, Y. H., Member, S., Waldteufel, P., Richaume, P., Wigneron, J. P., Member, S., Ferrazzoli, P., Member, S., Mahmoodi, A., Bitar, A. A., Cabot, F., Gruhier, C., Juglea, S. E., Leroux, D., Mialon, A., and Delwart, S.: The SMOS Soil Moisture Retrieval Algorithm, 50, 1384–1403, 2012.

Klein, L. and Swift, C.: An improved model for the dielectric constant of sea water at microwave frequencies, Oceanic Engineering, IEEE Journal of, 2, 104–111, doi:10.1109/joe.1977.1145319, 1977.

Kovacs, A.: Part I . Bulk Salinity Versus Ice Floe Thickness, 1996.

Kwok, R. and Cunningham, G. F.: ICESat over Arctic sea ice: Estimation of snow depth and ice thickness, Journal of Geophysical Research: Oceans, 113, 1–17, doi:10.1029/2008JC004753, 2008.

Laxon, S. W., Giles, K. A., Ridout, A. L., Wingham, D. J., Willatt, R., Cullen, R., Kwok, R., Schweiger, A., Zhang, J., Haas, C., Hendricks, S., Krishfield, R., Kurtz, N., Farrell, S., and Davidson, M.: CryoSat-2 estimates of Arctic sea ice thickness and volume, Geophysical Research Letters, 40, 732–737, doi:10.1002/grl.50193, 2013.

Lebedev: Rost l'da v arkticheskikh rekakh i moriakh v zavisimosti ot otritsatel'nykh temperatur vozdukha, 5-6 edn., 1938.

Leppäranta, M. and Manninen, T.: The brine and gas content of sea ice with attention to low salinities and high temperatures, 1988.

Lindsay, R. and Schweiger, a.: Arctic sea ice thickness loss determined using subsurface, aircraft, and satellite observations, The Cryosphere, 9, 269–283, doi:10.5194/tc-9-269-2015, http://www.the-cryosphere.net/9/269/2015/, 2015.

Maaß, N., Kaleschke, L., Tian-Kunze, X., and Drusch, M.: Snow thickness retrieval over thick Arctic sea ice using SMOS satellite data, The Cryosphere, 7, 1971–1989, doi:10.5194/tc-7-1971-2013, http://www.the-cryosphere.net/7/1971/2013/, 2013.

Maaß, N., Kaleschke, L., Tian-Kunze, X., and Tonboe, R. T.: Snow thickness retrieval from L-band brightness temperatures: a model comparison, Annals of Glaciology, 56, 9–17, doi:10.3189/2015AoG69A886, http://www.igsoc.org/annals/56/69/t69A886.html, 2015.

Maykut, G. and Untersteiner, N.: Some results from a time-dependent thermodynamic model of sea ice, Journal of Geophysical Research, http://onlinelibrary.wiley.com/doi/10.1029/JC076i006p01550/full, 1971.

Mecklenburg, S., Drusch, M., Y.H. Kerr, Font, J., Martin-Neira, M., Delwart, S., Buenadicha, G., Reul, N., Daganzo-Eusebio, E., and Oliva, R.: ESA ' s Soil Moisture and Ocean Salinity Mission - Mission overview and first results, Geophysical Research Abstracts, 13, 3628–3628, 2012.

Meier, W.: Actic sea ice in tranformation: A review of recent observed changes and impacts on biology, Reviews of Geophysics, 53, 1–33, doi:10.1002/2013RG000431.Received, 2015.

Menashi, J. D., St Germain, K. M., Swift, C., Comiso, J. C., and Lohanick, A.: Low-frequency passive-microwave observations of sea ice in the Weddell Sea., Journal of Geophysical Research: Oceans, 98, 22 569 – 22 577, http://onlinelibrary.wiley.com/doi/10.1029/93JC02058/full, 1993.

Peng, G., Meier, W. N., Scott, D. J., and Savoie, M. H.: A long-term and reproducible passive microwave sea ice concentration data record for climate studies and monitoring, Earth System Science Data, 5, 311–318, doi:10.5194/essd-5-311-2013, 2013.

Pounder, E.: The Physics of Ice, Pergamon Press, the Commonwealth and International Library, Geophysics Devision, Oxford, p. 151, 1965.

Reul, N., Fournier, S., Boutin, J., Hernandez, O., Maes, C., Chapron, B., Alory, G., Quilfen, Y., Tenerelli, J., Morisset, S., Kerr, Y., Mecklenburg, S., and Delwart, S.: Sea Surface Salinity Observations from Space with the SMOS Satellite: A New Means to Monitor the Marine Branch of the Water Cycle, Surveys in Geophysics, 35, 681–722, doi:10.1007/s10712-013-9244-0, 2014.

Ricker, R., Hendricks, S., Helm, V., Skourup, H., and Davidson, M.: Sensitivity of CryoSat-2 Arctic sea-ice freeboard and thickness on radar-waveform interpretation, Cryosphere, 8, 1607–1622, doi:10.5194/tc-8-1607-2014, 2014.

Ryvlin, A. I.: Method of forecasting flexural strength of an ice cover.No Title, Probl. Arct. Antarct, 45, 79–86, 1974.

Schwank Mike, Mätzler, C., Wiesmann, A., Wegmüller, U., Pulliainen, J., Lemmetyinen, J., Rautiainen, K., Derksen, C., Toose, P., and Drusch, M.: Snow Density and Ground Permittivity Retrieved from L-Band Radiometry: A Synthetic Analysis, IEE Journal of Selected Topics in Applied Earth Observations and Remote Sensing, 2015.

Semtner, A.: A model for the thermodynamic growth of sea ice in numerical investigations of climate, Journal of Physical Oceanography, http://journals.ametsoc.org/doi/abs/10.1175/1520-0485(1976)006{\T1\textless}0379:AMFTTG{\T1\textgreater}2.0.CO;2, 1976.

Spreen, G., Kaleschke, L., and Heygster, G.: Sea ice remote sensing using AMSR-E 89-GHz channels, Journal of Geophysical Research, 113, C02S03, doi:10.1029/2005JC003384, http://doi.wiley.com/10.1029/2005JC003384, 2008.

Stark, J. D., Ridley, J., Martin, M., and Hines, A.: Sea ice concentration and motion assimilation in a sea ice-ocean model, Journal of Geophysical Research: Oceans, 113, 1–19, doi:10.1029/2007JC004224, 2008.

Tian-Kunze, X., Kaleschke, L., and Maass, N.: SMOS Daily Polar Gridded Brightness Temperatures, [2012-2013], icdc.cen.uni-hamburg.de, 2012.

Tian-Kunze, X., Kaleschke, L., Maaß, N., Mäkynen, M., Serra, N., Drusch, M., and Krumpen, T.: SMOS-derived thin sea ice thickness: algorithm baseline, product specifications and initial verification, The Cryosphere, 8, 997–1018, doi:10.5194/tc-8-997-2014, http://www.the-cryosphere.net/8/997/2014/, 2014.

Tietsche, S., Balmaseda, M. A., Zuo, H., and Mogensen, K.: Arctic sea ice in the ECMWF MyOcean2 ocean reanalysis ORAP5, p. 33, http://old.ecmwf.int/publications/library/ecpublications/{_}pdf/tm/701-800/tm737.pdf, 2014.

Tietsche, S., Balmaseda, M. a., Zuo, H., and Mogensen, K.: Arctic sea ice in the global eddy-permitting ocean reanalysis ORAP5, Climate Dynamics, doi:10.1007/s00382-015-2673-3, http://link.springer.com/10.1007/s00382-015-2673-3, 2015.

Tilling, R. L., Ridout, a., and Shepherd, a.: Near Real Time Arctic sea ice thickness and volume from CryoSat-2, The Cryosphere Discussions, pp. 1–15, doi:10.5194/tc-2016-21, http://www.the-cryosphere-discuss.net/tc-2016-21/, 2016.

Tiuri, M. E.: The Complex Dielectric Constant of Snow at Microwave, IEEE Journal of Oceanic Engineering, 9, 377–382, 1984.

Ulaby, F. T., Moore, R. K., and Fung, A. K.: Microwave remote sensing.Active and passive., Kansas Univ.; Lawrence, KS, United States, http://ntrs.nasa.gov/search.jsp?R=19820039342, 1981.

Untersteiner, N.: Calculationsof TemperatureRegime and Heat Budget of Sea Ice in ,the Central Arctic, 69, 4755–4766, 1964.

Vant, M. R., Ramseier, R. O., and Makios, M.: The complex-dielectric constant of sea ice at frequencies in the range 0.1-40 GHz., Journal of Applied Physics, 49, 1264–1280, 1978.

Xie, J., Counillon, F., Bertino, L., Tian-kunze, X., and Kaleschke, L.: Benefits of assimilating thin sea ice thickness from SMOS into the TOPAZ system, The Cryosphere, 10, 2745–2761, doi:10.5194/tc-10-2745-2016, 2016.

Yu, Y. and Rothrock, D. a.: Thin ice thickness from satellite thermal imagery, Journal of Geophysical Research, 101, 25 753, doi:10.1029/96JC02242, 1996.

Zhang, J. and Rothrock, D. a.: Modeling Global Sea Ice with a Thickness and Enthalpy Distribution Model in Generalized Curvilinear Coordinates, Monthly Weather Review, 131, 845–861, doi:10.1175/1520-0493(2003)131<0845:MGSIWA>2.0.CO;2, 2003.

Zuo, H., Balmaseda, A. M., and Mogensen, K.: The new eddy-permitting ORAP5 ocean reanalysis: description, evaluation and uncertainties in climate signals, Climate Dynamics, pp. 1–21, doi:10.1007/s00382-015-2675-1, http://marine.copernicus.eu/services-portfolio/access-to-products/?option=com{_}csw{&}view=details{&}product{_}id=GLOBAL{_}REANALYSIS{_}PHYS{_}001{_}017, 2015.